Appl Petrochem Res (2017) 7:107–118
https://doi.org/10.1007/s13203-017-0182-5

ORIGINAL ARTICLE

Oxidative dehydrogenation of ethane with carbon dioxide over Cr_2O_3/SBA-15 catalysts: the influence of sulfate modification of the support

P. Thirumala Bai[1] · S. Srinath[1] · K. Upendar[2] · T. V. Sagar[2] · N. Lingaiah[2] · K. S. Rama Rao[2] · P. S. Sai Prasad[2]

Received: 11 January 2017 / Accepted: 7 September 2017 / Published online: 20 September 2017

Abstract Unmodified and sulfate-modified SBA-15-supported Cr_2O_3 catalysts were prepared by impregnation method. The physico-chemical properties of the supports and catalysts were determined by nitrogen adsorption/desorption, powder X-ray diffraction (XRD), Fourier transform infrared spectroscopy (FT-IR), laser-Raman spectroscopy, X-ray photoelectron spectroscopy (XPS), UV–Vis diffuse reflectance spectroscopy (UV-DRS), inductively coupled plasma optical emission spectroscopy (ICP-OES), transmission electron microscopy (TEM) and temperature-programmed reduction (TPR) techniques. Oxidative dehydrogenation of ethane to ethylene (ODE) with CO_2 as oxidant was carried out on these catalysts in a fixed-bed reactor at temperatures in the range of 600–700 °C and at atmospheric pressure. The changes in structural and textural properties because of sulfate modification were identified. Sulfate modification affected the nature of interaction of CrO_x species with the SBA-15 support. During the evaluation, it was observed that sulfate modification enhances ethane conversion and ethylene selectivity of the catalyst. Better dispersion of CrO_x and the increase in Cr^{6+}/Cr^{3+} ratio seem to be the reasons for the higher performance of the sulfate-modified catalysts compared to that of the unmodified catalyst.

✉ P. S. Sai Prasad
saiprasad@iict.res.in

[1] Department of Chemical Engineering, National Institute of Technology, Warangal, India

[2] Inorganic and Physical Chemistry Division, Indian Institute of Chemical Technology, Hyderabad 500 007, India

Keywords Oxidative dehydrogenation of ethane · Carbon dioxide · Chromium oxide · Ethane · Ethylene · Sulfated SBA-15

Introduction

Ethylene is an important raw material for the synthesis of plastics, fibers and other organic chemicals. Its production capacity reached 160 million tons in 2015. One of the methods of producing ethylene is steam cracking of hydrocarbons. However, this endothermic reaction is highly energy intensive necessitating very high operating temperatures. Besides, coking is a major disadvantage of this process. Recently, catalytic oxidative dehydrogenation of ethane (ODE) using oxygen as the oxidant has emerged as an alternative to thermal cracking. ODE offers the advantages of decreasing the operating temperature and making the reaction exothermic instead of endothermic [1]. The literature on ODE with oxygen is now abundant with many reports proposing various catalysts [2, 3]. However, this mode of operation necessitates a separate facility for oxygen generation, and secondly it is difficult to achieve high ethylene selectivity due to uncontrolled CO_x formation [4]. CO_2 is identified as a better oxidant because of its mild oxidation nature and its advantage in moderating the exothermicity of the reaction [5]. Chromium-based catalysts are found to be highly active and selective for the ODE with CO_2. Al_2O_3, SiO_2, TiO_2 and ZrO_2-supported Cr_2O_3 catalysts are studied to elucidate the dependence of catalytic activity on the distribution of CrO_x and the structure of CrO_x species on the surface [6]. The influence of the nature of oxidant (O_2 or CO_2) on the performance of the catalysts is also reported [7, 8]. Compared to oxygen, CO_2 in the feed is shown to facilitate the dehydrogenation

activity by enhancing ethane conversion, apart from increasing ethylene yield and retarding coke deposition on the catalyst significantly [9]. The chromium in its high oxidation state, such as Cr^{6+} on the surface, is observed to be the active species [10]. Reducibility is another parameter that decides the rate of ethane dehydrogenation, as reported in the case of Cr–O and Cr–V–O oxide catalysts [1]. Thus, the selection of catalyst that gives higher conversion of ethane and high selectivity towards ethylene has been the focus of the studies.

SiO_2 is the most favored support for the chromia catalysts. 5–8 wt% Cr_2O_3/SiO_2 catalysts have exhibited excellent performance [6, 11]. However, the aggregation of CrO_x on SiO_2 is found to negatively influence the catalyst behavior, particularly during the reaction on Cr–Si-2 molecular sieve catalyst [12]. SBA-15 is later found to be a convenient support to overcome the problem of aggregation [13]. Wang et al. reported that sulfate modification of the silica support is advantageous for the preparation of highly active chromia catalysts for the ODE reaction in the presence of CO_2 [14]. While highlighting the importance of silica, the influence of the presence of strong basic promoters (alkali metal oxides) in suppressing the catalytic activity is also reported [15]. Sulfate modification of zirconia was attempted in studies related to ODE to achieve better results [16]. An intensive observation of the literature reveals that though the benefits are elaborated, the reasons for the better performance of the sulfate-modified catalysts are not reported. Particularly, the influence of sulfate modification of the support in Cr_2O_3/SBA-15 has not been studied. In this communication, we report the effect and the reasons for the enhanced activity and selectivity in the case of Cr_2O_3 supported on sulfate-modified SBA-15 catalyst.

Experimental

Preparation of catalysts

SBA-15 was synthesized adopting the procedure described in the literature [17]. In a typical experiment, 20 g of triblock copolymer (P123, Aldrich) was dispersed in a solution prepared by taking 465 mL of distilled water and 137.5 g of 35% hydrochloric acid (M/s. Loba Chemie). 44 g of tetraethyl orthosilicate (TEOS, Aldrich) was added to this solution under constant stirring at 40 °C and the mixture was subjected to hydrothermal treatment at 100 °C for 24 h. The resultant slurry was filtered, dried in air at 110 °C for 12 h, and then calcined in air at 550 °C for 4 h. For the 6 wt% sulfate modification, the SBA-15 was impregnated with required quantity of aqueous ammonium sulfate solution (sample denoted as S.SBA-15). 5 wt% Cr_2O_3/SBA-15 (Cr/SBA-15) and 5 wt% Cr_2O_3/sulfated SBA-15 (Cr/S.SBA-15) were prepared by impregnating the supports with required quantities of aqueous chromium nitrate (Wako Chemicals) solution. For the above three catalysts, the impregnation step was followed by drying at 120 °C and calcination at 700 °C for 4 h [17].

Catalysts characterization

BET surface area, pore volume and average pore diameter were determined by N_2 adsorption/desorption, using the BET and BJH equations, respectively, on a SMART SORB 92/93 instrument. Prior to the measurement, the samples were dried at 150 °C for 2 h and the adsorption/desorption was followed using nitrogen at liquid nitrogen temperature. XRD patterns of the catalysts were obtained on an Ultima-IV diffractometer (M/s. Rigaku Corporation, Japan) using nickel-filtered Cu Kα radiation ($\lambda = 1.54$ Å). The measurements were recorded in steps of 0.045° with count time of 0.5 s in the 2θ range of 0–80°. Identification of the crystalline phases was carried out with the help of JCPDS files. H_2-TPR studies were performed using a home-made apparatus. Catalyst samples (50 mg) taken in a quartz reactor were reduced under 10% H_2/Ar gas mixture at a flow rate of 30 mL/min and a heating rate of 5 °C/min up to 800 °C. Before the TPR run, the catalysts were pretreated in argon flow at 300 °C for 2 h. Hydrogen consumption was monitored using thermal conductivity detector of a gas chromatograph (Varian, 8301). UV–Vis DRS spectra of the catalyst samples were recorded on a GBC Cintra 10e UV–visible spectrometer in the region of 200–800 nm, with a split width of 1.5 nm and scan speed of 400 nm per minute. 15 mg of the catalyst sample mixed with an appropriate quantity of dry KBr was ground thoroughly for making the pellet to extract the FT-IR spectra at room temperature on a Perkin Elmer (M/s. Spectrum GX, USA) instrument. XPS studies were performed on a Thermo K-5 Alpha XPS instrument at a pressure better than 1×10^{-9} torr. The Cr2p and O1s core-level spectra were recorded using Al Kα radiation (photon energy = 1253.6 eV) at a pass energy of 50 eV. The core-level binding energies (BEs) were charge corrected with respect to the adventitious carbon (C1s) peak at 284.6 eV. Raman spectra were recorded on a LabRam HR800UV Raman spectrometer (Horiba Jobin-Yvon) attached with a confocal microscope and liquid nitrogen cooled charge coupled device detector. The chemical analysis of the chromia containing samples was carried out by inductively coupled plasma optical emission spectroscopy (ICP-OES) using a Varian 725ES instrument. The morphological analysis of these samples was also carried out using transmission electron microscopy (TEM on a JEOL 100S microscope). For the preparation of a sample for TEM, a suspension

containing about 1 mg catalyst/mL of ethanol was prepared and sonicated for 10 min. A few drops of the suspension were placed on a hollow copper grid coated with a carbon film.

Activity test

The performance of the catalysts was evaluated in a fixed-bed reactor at atmospheric pressure. A mixture of He/C_2H_6/CO_2 at a ratio of 27/9/54 was used as the feed. The activity tests were carried out using 0.5 g of catalyst suspended between two quartz wool plugs in the reactor. Ceramic beads of the same weight were used for diluting the catalyst. The catalyst was first preheated in a flow of He at 30 mL/min at 500 °C for 4 h. The activity tests were conducted in the temperature range of 600–700 °C. The analysis of the reaction product was carried out online using a Nucon 5765 gas chromatograph equipped with a Porapak-Q column. He gas carrier and a thermal conductivity detector (TCD) were used for analysis. After the reaction reached steady state over a period of 1 h, the product analysis was duplicated and the average value considered. The accuracy was within the error margin of ±3%.

Results and discussion

BET surface area, pore volume and pore diameter

The estimated values of BET surface area, pore volume and pore diameter along with the Cr_2O_3 wt% of the catalysts are reported in Table 1. There is a decrease in surface area and pore volume after sulfation of SBA-15. However, the decrease is more after the addition of CrO_x to SBA-15. The formation of extra-framework CrO_x species with lower surface area might be the reason for the decrease in the specific surface area of SBA-15, as also reasoned by Zhang et al. [18]. One important observation from these results is that prior addition of sulfate ion to the support reduces the loss in surface area due to CrO_x addition.

Pore size distribution patterns of the samples are shown in Figs. 1 and 2. The H1-type hysteresis loop of SBA-15

Table 1 Textural characteristics of the supports and catalysts

Catalysts	S_{BET} (m^2/g)	V_p (cm^3/g)	D_{BJH} (nm)	Cr_2O_3 composition (wt%)
SBA-15	506	0.681	6.6	–
S.SBA-15	462	0.671	6.5	–
Cr/S.SBA-15	435	0.648	5.9	4.92
Cr/SBA-15	417	0.645	5.8	4.85

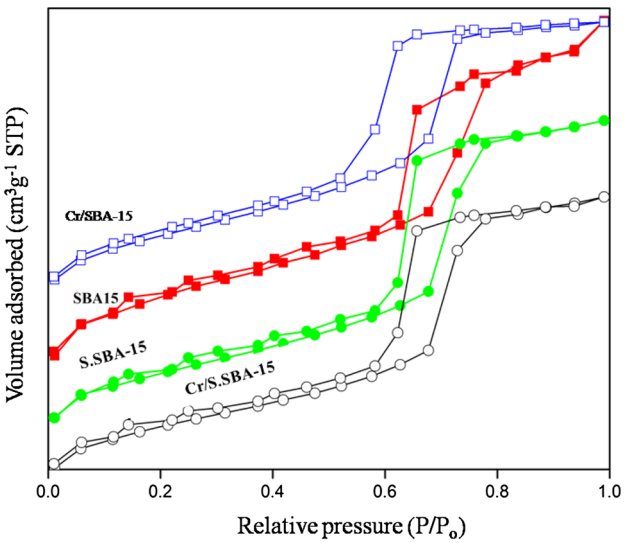

Fig. 1 N_2 adsorption/desorption isotherms of the supports and catalysts

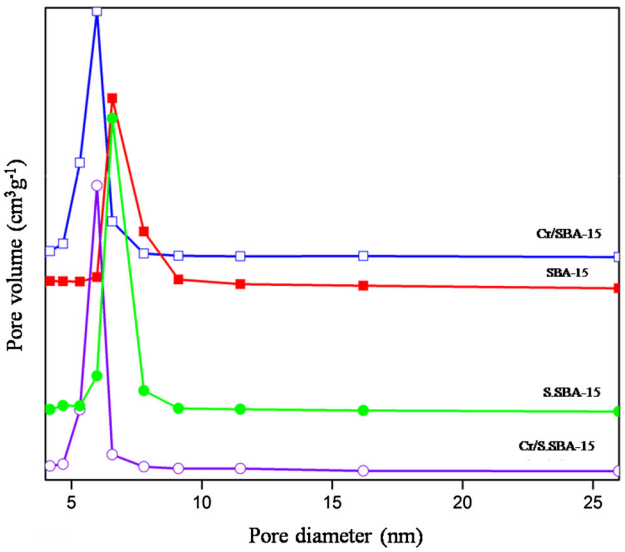

Fig. 2 Pore size distribution of the supports and catalysts

confirms the mesoporous structure of material with cylindrical channels [17]. A sharp inflection is observed at the relative pressure of $p/p_o = 0.6–0.8$ corresponding to capillary condensation within uniform mesopores. The isotherms of Cr/SBA-15 and Cr/S.SBA-15 also show similar patterns revealing the intactness of the hexagonally ordered structure. The non-closure of the adsorption and desorption patterns can be seen from the figure, which may be explained as follows. Esparza et al. [20] have reported, SBA-15 materials may contain some amount of intra-wall pores that can possibly interfere adsorption/desorption phenomenon. In addition to this, a sort of pore-blocking effect occurs if the cross section of the pore varies along its length. Instead of following an ideal desorption mechanism

in which a pore of a given diameter releases completely its condensate at a particular relative pressure, the emptying of pore in SBA-15 substrates takes place progressively rather than abruptly. The decrease in pore volume is due to partial blockage of the mesopores of SBA-15 after anchoring of CrO_x species on to the surface. During this process some pore wall collapse might have taken place in the SBA-15 structure leading to the decrease of the pore diameter, as reported by Shi et al. [19]. The phenomenon of non-closure of adsorption and desorption can be observed from the isotherms which can be explained as follows.

XRD results

Figure 3a shows the low-angle XRD patterns of SBA-15, sulfate-modified SBA-15 supports and the unmodified and sulfate-modified catalysts. The peaks at 2θ values of 0.98°, 1.74°, and 2.00° can be indexed as (100), (110), and (200) reflections which are associated with p6 mm hexagonal symmetry of SBA-15 [17]. These profiles confirm the presence of typical hexagonally structured SBA-15 with highly ordered mesoporous channels even after CrO_x impregnation before and after sulfate modification [17]. The addition of CrO_x to SBA-15 shows a small right shift towards high 2θ region. On the other hand, the sulfate-modified SBA-15 shows no deviation. The shift in the case of Cr/SBA-15 catalyst may indicate partial substitution of Si with Cr species in the SBA-15 frame work. However, the isomorphic substitution of Si^{4+} (ionic radius of 0.40 Å) with Cr^{3+} (ionic radius of 0.62 Å) is difficult. The Cr^{6+} (ionic radius of 0.44 Å) can be substituted resulting in an increase in lattice parameter of SBA-15. But the extent of isomorphic incorporation of metal ions into the silica framework is low because of the problem with the dissolution of metal ions in the solution at very low pH. Therefore, the shift in the peak position that indicates the increase in unit cell constant may be considered trivial in the case of Cr/SBA-15, as also opined by Charan et al. [21]. Instead, the shift in the d_{100} peak to a higher angle may be attributed to the blockage the frameworks of SBA-15 after the interaction of CrO_x species [21].

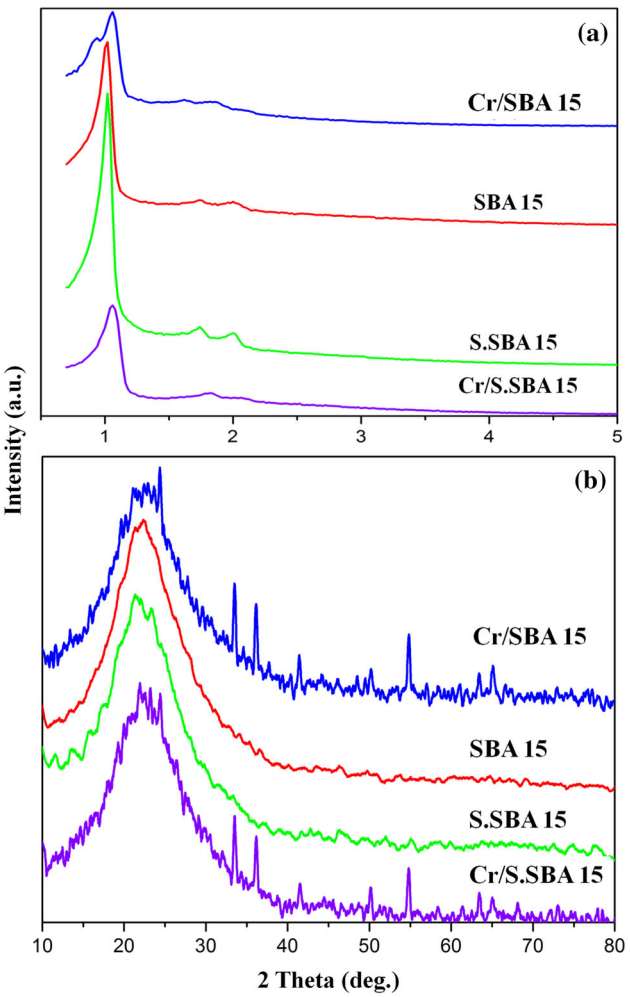

Fig. 3 XRD patterns of the supports and catalysts: **a** low angle and **b** wide angle

The wide-angle XRD patterns of catalysts are depicted in Fig. 3b. SBA-15 exhibits a broad peak between 15° and 30° which is characteristic of amorphous silica [19]. The diffraction patterns of CrO_x-containing catalysts show peaks at $2\theta = 24.38°$, 33.50°, 36.16°, 41.42°, 50.18°, 54.84°, 63.42° and 65.10° ascribed to the presence of crystalline Cr_2O_3 (JCPDS No.: 84-1616) [22]. The intensities of these peaks are lower in Cr/S.SBA-15 catalyst than those of Cr/SBA-15 indicating better dispersion of the CrO_x species in the modified catalyst. This result suggests that the addition of sulfate ion obviously enhances the dispersion of the chromium species in the Cr/S.SBA-15 catalyst.

FT-IR results

FT-IR spectra of the catalyst samples are presented in Fig. 4. The vibrational bands at 3400, 1632–1640, 1055–1213, 958, 805–809, 566–575 and 460–489 cm^{-1} correspond to the surface silanols; Si–O–Si, Si–O and the hydrated Si–O groups [23]. The symmetric stretching modes of Si–O–Si groups are observed at around 796 cm^{-1}. The peak at 455 cm^{-1} is assigned to bending vibration of Si–O–Si groups, while the adsorption bands at 967 and 3398 cm^{-1} correspond to defective Si–OH groups [23]. The high wavelength (3567 cm^{-1}) absorption bands are due to –OH stretching in intermolecular water. The bands at 1080 and 1227 cm^{-1} correspond to Si–O asymmetric stretching, internal and external, respectively, whereas the one at 800 cm^{-1} (Si–O symmetric stretching)

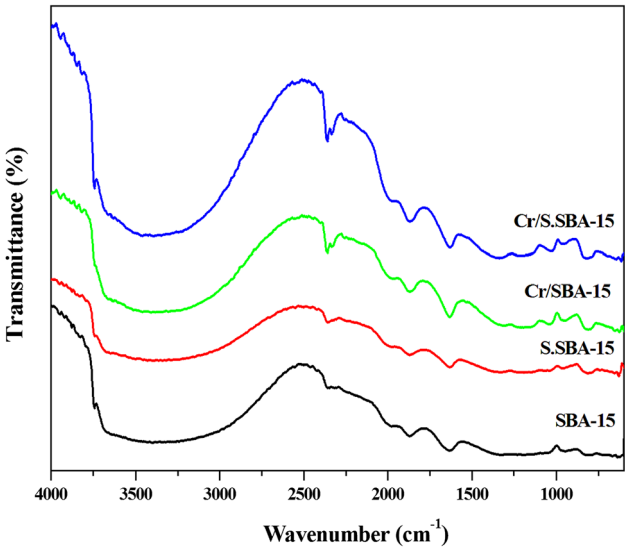

Fig. 4 FT-IR spectra of supports and catalysts

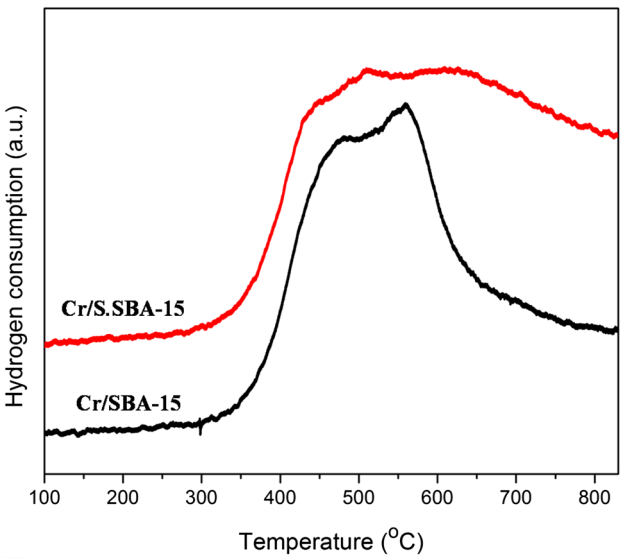

Fig. 5 TPR profiles of the catalysts

is due to SiO_4 vibrations [24] in the SBA-15 frame work. 1632–1640 cm^{-1} bands are ascribed to the Si–O stretching overtone and or adsorbed water. Like SiO_2, SBA-15 has a covalent framework which can be severely hydroxylated. It can predominantly stabilize isolated (single), $(O)_3$–Si–OH and geminal $(O)_2$–Si–$(OH)_2$ silanol groups on its surface. These surface silanol groups are imperative for grafting chromia species to SBA-15 [21]. The bands at 573 and 620 cm^{-1} are due to extra-framework hydrated CrO_x species present on the pore surfaces [21, 22]. Especially, the intense band at 573 cm^{-1} in the sample indicates the existence of Cr-polycation. A close observation of intensities of the bands at 550 and 620 cm^{-1} seen in Cr/SBA-15 and Cr/S.SBA-15 catalysts indicate that there is a decrease in intensity of 550 cm^{-1} band after sulfate modification. Thus, there is a more prevalence of hydrated CrO_x species in the latter indicating better dispersion [25]. The FT-IR spectra show weak bands at 2344–2365 and 1856 cm^{-1} corresponding to the C–O and C=O stretching vibrations, respectively.

TPR results

TPR analysis provides valuable information regarding the redox property of a catalyst. The TPR profiles of the CrO_x-containing catalysts are displayed in Fig. 5. These samples show complex reduction profiles. Several discrepancies in H_2-TPR analysis of CrO_x are reported in the literature [22]. The reduction profiles of CrO_x depend on parameters such as method of preparation, calcination temperature, support material, nature of interaction of CrO_x with supports and the type of chromium species (dispersed mono or polychromates) grafted on to the surface. The nature of Cr oxidation state strongly depends on the strength of interaction between CrO_x and SBA-15 through the surface silanol groups. Cr/SBA-15 shows a strong reduction band at 550 °C with shoulder at 450 °C due to the reduction of chromium species from $Cr^{6+} \rightarrow Cr^{3+}$ [26, 27]. Sulfate modification has shifted the reduction maxima to higher temperatures. The higher reduction temperature observed in Cr/S.SBA-15 in comparison with that of Cr/SBA-15 suggests that there is a stronger interaction leading to better dispersion of CrO_x species in the former case [14].

Earlier studies revealed that the Cr ions exist in various oxidation states in supported chromium materials, in which Cr^{6+} and Cr^{3+} are prominent in redox processes in the catalytic oxidative dehydrogenation of alkanes [13, 28, 29]. Cavani et al. [30] have reported the formation of two kinds of Cr^{6+} species, the grafted and the soluble. The grafted Cr^{6+} species, which is anchored to the silica surface, has a greater interaction with the silica support and is harder to be reduced than the soluble Cr^{6+} species, which presents as isolated chromates on the surface of the catalyst. Therefore, the intense peak at lower temperature (ca. 374–397 °C) corresponds to reduction of soluble Cr^{6+} species, and the one at higher temperature (ca. 510 °C) results from reduction of the grafted Cr^{6+} species. It has been reported that for chromium oxides deposited on the zeolite or oxide materials, a higher temperature is needed to reduce the highly dispersed Cr species.

UV-DRS results

The UV–Vis DRS patterns (Fig. 6) have shown absorbance bands at 250, 350, 450 and 600 nm. According to literature the lower wavelengths at 250, 350 and 450 nm are due to

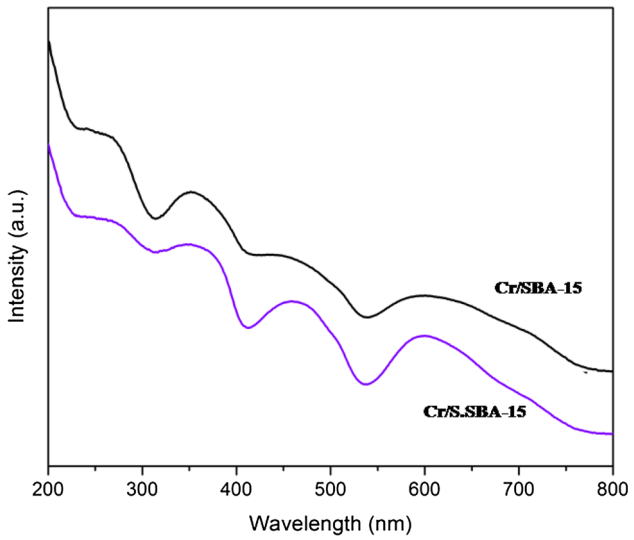

Fig. 6 UV-DRS bands of the catalysts

the presence of monochromatic Cr^{6+} species. 250 and 350 nm bands are due to the charge transfer spectra of *d–d* transitions from 1A1 → 1T2 transitions of tetrahedral Cr-oxide. 450 nm bands are due to the symmetric forbidden nature of transitions from 1A1 → 1T1 of tetrahedral Cr-oxides. On the other hand, the 600 nm bands are due to the symmetric transitions of A2g → T2g octahedral coordinated Cr^{3+} in Cr_2O_3 clusters [26, 31]. The results indicate that Cr^{6+} species of mono- and polychromate are dominant in Cr/S.SBA-15.

XPS results

O1s XPS Figure 7 shows the O1s spectra of all catalysts. The peaks observed correspond to the BE varying in the range of 534–536 eV for O1s. SBA-15 shows peaks at 534.3 and 535.8 eV, the addition of sulfate ion shows a high BE value than the parent SBA-15 indicating the interactions of sulfate with SBA-15. The high-energy features are observed as a result of the energy loss due to the interaction of O1s photoelectrons with the electrons in the surface region of the SBA-15 walls. CrO_x addition to SBA-15 shows a left shift in the BE values describing their stronger interaction with SBA-15. Literature reveals [22] that the shift of O1s peak position towards lower binding energy indicates the possible generation of CrO_x domains on CrO_x/SBA-15 sample when the Cr surface density is $\geq$1.11 Cr-atom/nm^2 where there is the appearance of crystalline Cr_2O_3 phase. Therefore, we can assume high interaction of CrO_x with S.SBA-15 in the present case.

Cr2p XPS An investigation on the oxidation states of Cr ions is beneficial for the elucidation of the nature of the active sites in the catalysts. The results of Cr2p XPS studies

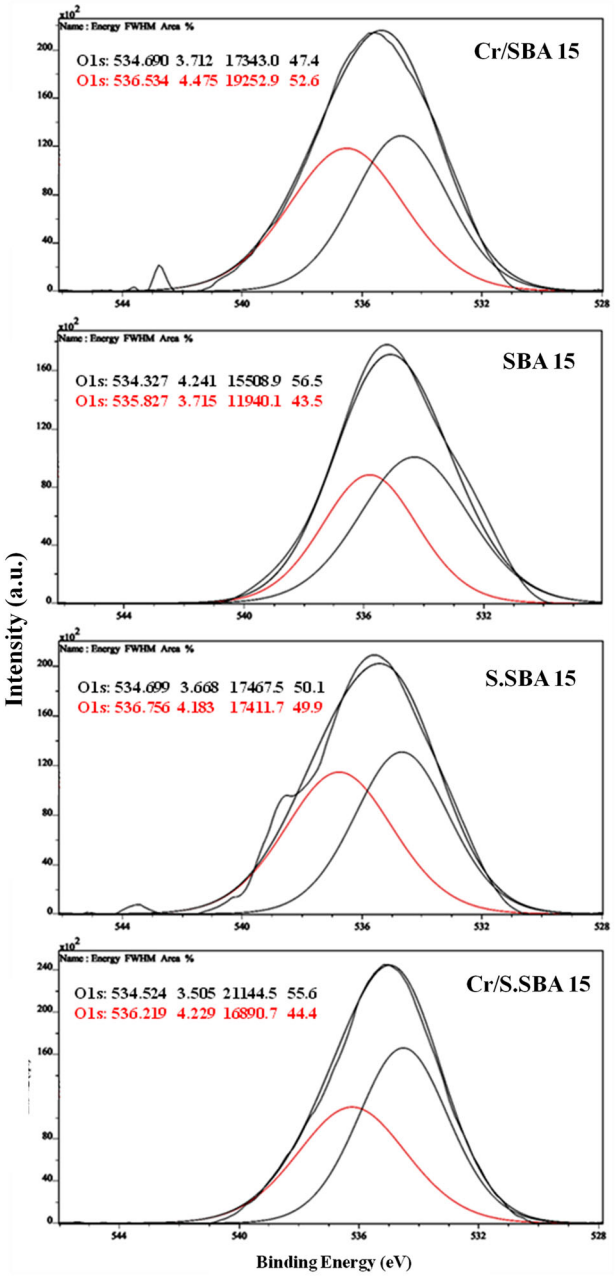

Fig. 7 O1s XP spectra of the catalysts

are presented in Fig. 8. The study establishes the formation of Cr^{6+} species in both the Cr containing catalysts. The asymmetric peaks spanning between BE of 575–580 and 585–589 eV could be deconvoluted into two sets of components; one set with BEs at 577 and 579 eV and the other at 586 and 588 eV. The former set of Cr2p signals can be assigned to Cr^{3+} ions, whereas those of the second set to Cr^{6+} ions. Thus, the peaks confirm the co-presence of Cr^{3+} and Cr^{6+} ions, as also reported in the literature [31, 32]. The peaks assigned to Cr^{6+} are more intense than those of Cr^{3+} indicating the dominance of Cr^{6+}, as also evidenced

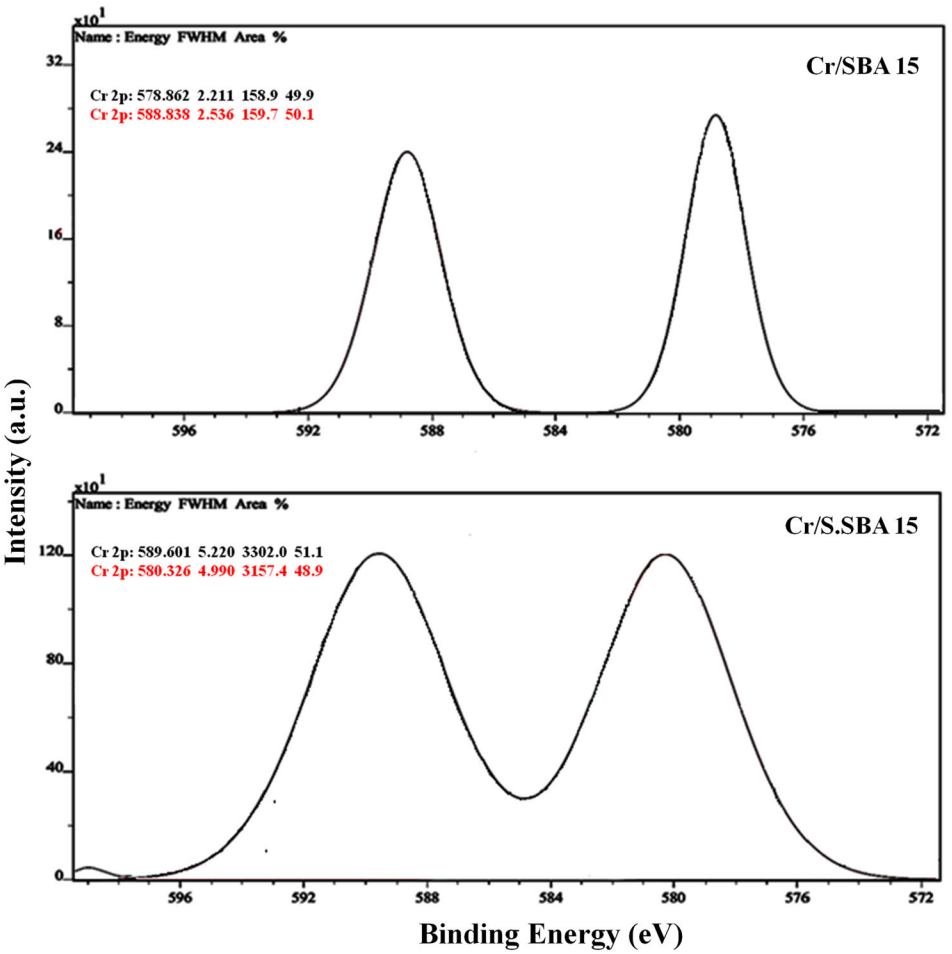

Fig. 8 Cr2p XP spectra of the catalysts

by the UV–Vis DRS studies. Sulfate ion addition helps promote chromium with higher oxidation states [33]. Since XPS is a surface technique, it is not possible to estimate the overall quantity of Cr^{6+} and Cr^{3+} species. However, a surface Cr^{6+}/Cr^{3+} ratio >1 can be discerned from the analysis which is preferable for the catalyst to show higher activity. These results are in good agreement with the X-ray diffraction results.

Laser-Raman results

In order to investigate the nature of chromium ion present on the SBA-15 support, Raman spectroscopy was employed. Raman spectra of catalysts are displayed in Fig. 9. Typically three kinds of Cr species, i.e., isolated monochromate, polychromate, and crystalline Cr_2O_3 are seen in supported chromia catalysts. The Raman spectrum of SBA-15 shows three bands at 497, 607 and 977 cm^{-1} assigned to cyclic tetrasiloxane rings, cyclic trisiloxane rings and the Si–OH stretching mode, respectively [34]. It can be seen that the spectra of chromium-incorporated samples exhibit a band at 987 cm^{-1} assigned to the

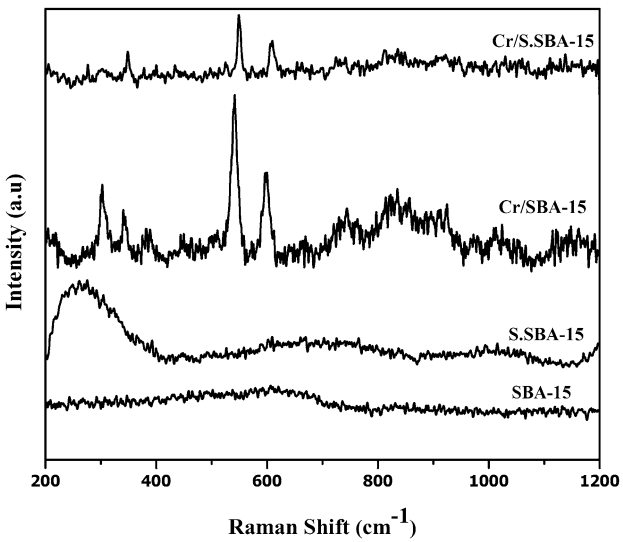

Fig. 9 Raman spectra of the support and catalysts

υ_s(O=Cr=O) stretching, the other at 394 cm^{-1} due to δ(O=Cr=O) bending, and finally, the band at 1014 cm^{-1} referred to υ(O=Cr=O) stretching, as reported by Dines

et al. during their DFT calculations [35]. Cr/SBA-15 shows several Raman bands appearing at 219, 306, 344, 394, 449, 505, 543, 601, 669, 747, 818–859, 915, 1014 and 1145 cm^{-1}. The Raman spectrum of Cr/S.SBA-15 shows bands at 353, 551, 606, 725, 814, 833, 908–945, 1057 and 1141 cm^{-1}, in which the band at 353 cm^{-1} could be ascribed to Cr^{6+} [36]. The peaks observed at 396, 929–949 cm^{-1} are attributed to monochromatic Cr^{6+} species [36, 37]. The Raman bands at 896 (weak), 970 (strong), and 1061 (weak) cm^{-1} can be attributed to Cr^{6+} species [22] and the band at 970 cm^{-1} is smaller in Raman shift than that at 980 cm^{-1} which is due to the Cr–O stretching of monochromate species in Cr-SBA-15 [31, 38]. The peaks in the range 690–1017 cm^{-1} are due to the polychromatic Cr^{6+} species from the oligomerization [31, 36]. Incorporation of sulfate ions in SBA-15 support is more favorable to formation of Cr^{6+} ion species than the unmodified one. These results corroborate the XRD analysis.

ICP-OES results

The composition of Cr_2O_3 present in the modified SBA-15 samples was determined by ICP-OES technique. The acquired results are presented in Table 1. These values are found to be very close to the theoretical values.

TEM results

The TEM micrographs of the Cr/SBA-15 and Cr/S.SBA-15 catalysts are shown in Fig. 10. The hexagonal structure of SBA-15 was confirmed by the TEM. The average crystal size of sulfate-modified catalyst was found to be 120 nm (Cr/S.SBA-15), whereas that for Cr.SBA-15 catalyst was 240 nm. From the above results, it can be concluded that modification with sulfate ion leads to decrease in crystal size.

Catalytic activity

All the catalysts were evaluated for their ODE performance using CO_2 as the oxidant. The CrO_x-containing catalysts show (Fig. 11a) high conversion of ethane and high ethylene selectivity and yield compared to the bare SBA-15 and S.SBA-15 supports. Cr/S.SBA-15 shows the highest conversion (61.2%) and selectivity (82.2%) in the series, with ethylene yield reaching 50.3%; the same for Cr/SBA-15 are obtained as 45.3, 76.9 and 36.5%, respectively. Thus, sulfate modification has a distinct influence of the performance of the catalysts. Better dispersion of Cr species on the sulfated sample might have increased ethane activity by facilitating more number of active sites, as also reported by Wang et al. [14].

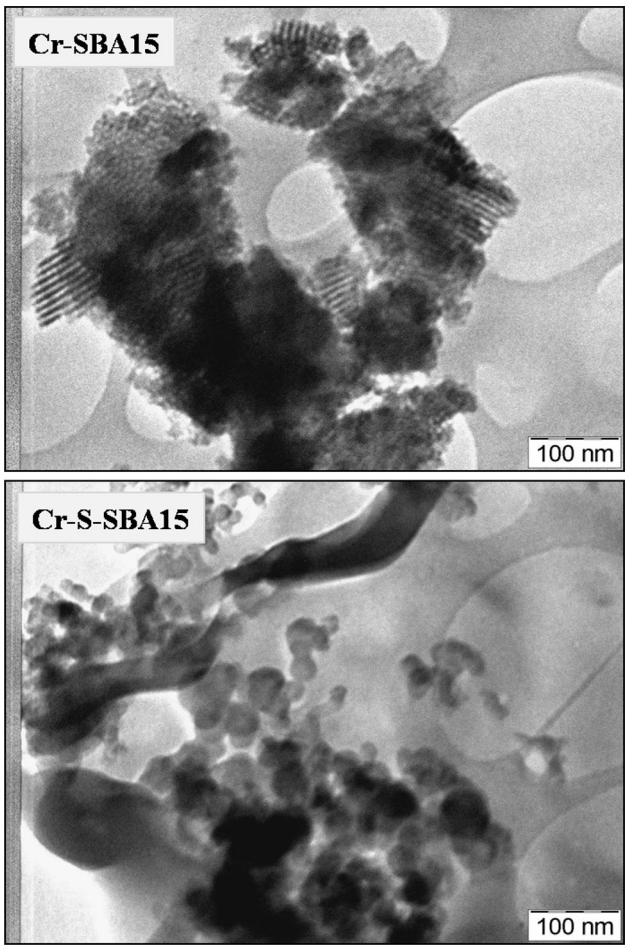

Fig. 10 TEM images of the catalysts

The chromium species with the high oxidation state is found to play a key role in obtaining higher catalytic activity during the dehydrogenation of light alkanes [39, 40]. Ge et al. [11] used electron spin resonance and UV-DRS to explore the active site for the ODE with CO_2 over silica-supported chromium oxide catalysts and established that the species with a higher oxidation state (Cr^{5+} or Cr^{6+}) is significant for the reaction. In the case of Cr/H-ZSM-5 (SiO_2/Al_2O_3 >190), Cr^{6+} or possibly Cr^{5+} was observed to be the active species. Fridman et al. investigated the CrO_x/Al_2O_3 catalyst for the dehydrogenation reaction and successfully identified chromium species which is responsible for the redox reaction [41, 42]. In the present catalysts also, the Cr^{6+} species seems to be responsible for the high activity of catalysts in the ODH of ethane with CO_2. The Cr^{6+} species is initially reduced to Cr^{3+} species during the dehydrogenation of ethane. Subsequently, the reduced Cr^{3+} is re-oxidized to Cr^{6+} species by CO_2, as described by the following equations [10]:

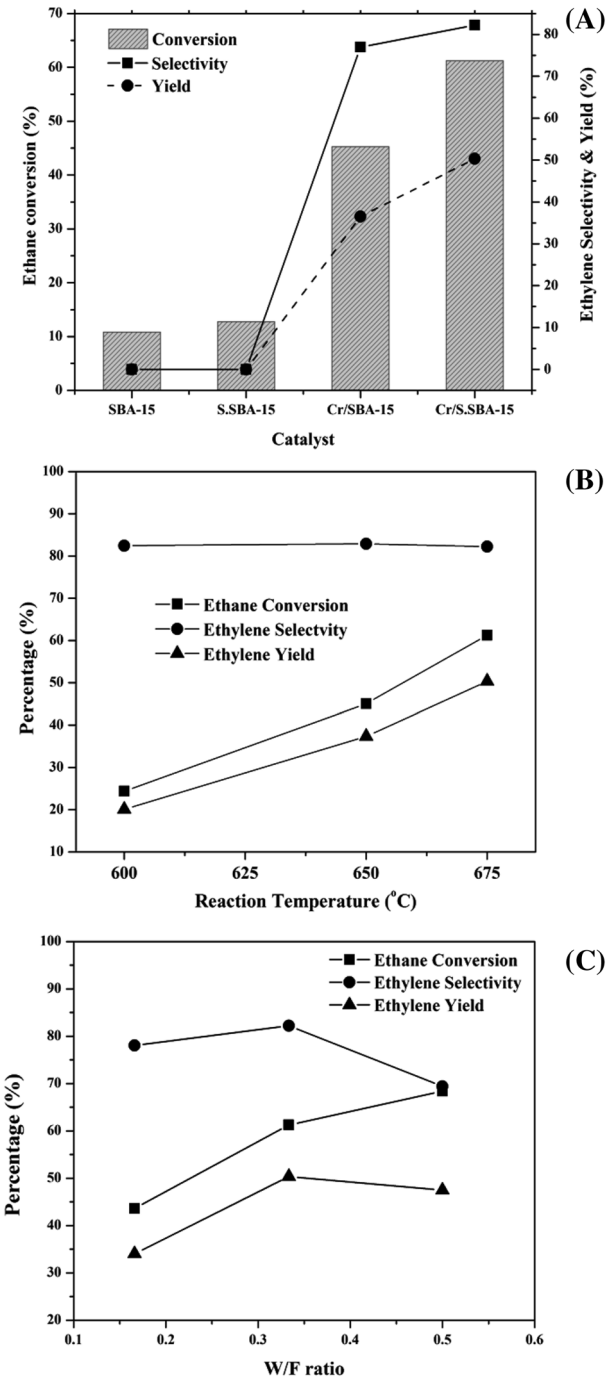

Fig. 11 **a** Activity of the catalysts; **b** effect of reaction temperature on the activity of Cr/S.SBA-15 catalyst; **c** catalytic performance of Cr/S.SBA-15 at different *W/F* ratios (temperature 675 °C; flow rate 9 mL/min ethane + 54 mL/min CO_2 + 27 mL/min He)

$$C_2H_6 + Cr^{6+} = O \rightarrow C_2H_4 + H_2O + Cr^{3+}$$
$$Cr^{3+} + CO_2 \rightarrow CO + Cr^{6+}.$$

8 wt% Cr_2O_3/SiO_2 catalyst exhibited an excellent performance producing 55.5% ethylene yield at 61% ethane conversion at 650 °C [6]. Ge et al. studied a series of silica-supported chromium oxide catalysts and found 5% Cr/SiO_2 catalyst exhibiting 30.7% ethane conversion and 96.5% ethylene selectivity at 700 °C. The high valent states of chromia (Cr^{5+} and/or Cr^{6+}) were observed to be important for the reaction [11]. Cr–Si-2 molecular sieve catalyst with 1.28 wt% chromium gave 45.5% ethylene yield with a selectivity of 87.9% at 650 °C. The change of Cr from a higher oxidation state to lower oxidation state was found to influence the catalyst behavior [12]. The ODH of ethane with CO_2 was successfully carried out over the Cr-based catalysts prepared by using FeCrAl alloy foil as support [13]. 66.5% ethane conversion and 99.5% ethylene selectivity were reported on the 5 wt% Cr-loaded monolithic catalyst at 750 °C. The reduction–oxidation cycle between Cr^{6+} and Cr^{3+} species was thought to be carried out via the dehydrogenation of ethane and oxidation by CO_2. Interactions between Cr, SBA-15, and the Al_2O_3/FeCrAl support modified the redox properties of the Cr/SBA-15/Al_2O_3/FeCrAl catalysts. The effect of Ce on the activity of Cr/SBA-15 catalyst was studied. An enhancement in the activity was observed after Ce modification. The Cr^{6+} to Cr^{3+} redox cycle was carried out by the sequential dehydrogenation of ethane and oxidation by CO_2 [19]. In the present investigation, FT-IR, UV-DRS, Raman and X-ray photoelectron spectroscopic investigations have revealed that the surface Cr species are mainly Cr^{6+} in mono and polychromate forms, with a minor amount of Cr^{3+}. The TPR profiles reveal the facile redox nature of Cr^{6+} to Cr^{3+}. The performance of the present catalyst is also comparable with those reported in the literature, except for small discrepancies due to the variation in the reaction temperature or the definition adopted for arriving at parameters. Thus, we believe that the predominance of surface Cr^{6+} species on the sulfate-modified catalyst also seems to be responsible for the higher activity. Smaller particles, presence of the greater number of active Cr^{6+} species and monolayer coverage of CrO_x with uniform dispersion on the support are responsible for the good performance of the catalyst. Better redox property due to higher oxidation state of chromium over the catalyst also leads to better performance.

The Cr^{6+}/Cr^{3+} ratio is also a significant factor in the ODH of ethane. Asghari et al. [43] reported a direct correlation between this ratio and the activity in their studies on MCM-41-supported Cr_2O_3 catalysts. The ratio increased up to 8% Cr where the activity was also maximum. Mimura et al. [10] proposed the nature of active species and the role of CO_2 in the ODH of ethane over Cr/H-ZSM-5 catalyst. The importance of the existence of a redox cycle involving Cr^{6+}/Cr^{3+} species is stressed. The high dehydrogenation activity can be obtained by the Cr redox cycle during the ODH of ethane in the presence of CO_2 [13].

The effect of reaction temperature on the activity and selectivity of Cr/S.SBA-15 catalyst is shown in Fig. 11b. It

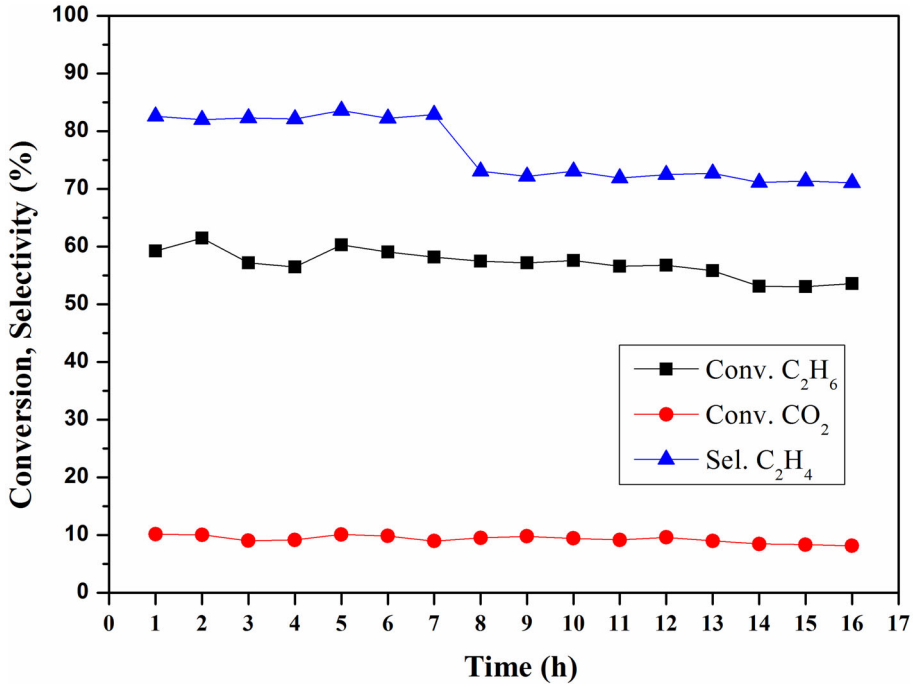

Fig. 12 Time on stream study of Cr_2O_3/S.SBA-15 catalyst

may be observed that with increase in reaction temperature the conversion of ethane increased and the selectivity continued to be at its high value. 675 °C is the best temperature in the studied region. The effect of space velocity on the ODE activity of Cr/S.SBA-15 was studied at 675 °C temperature and the results are disclosed in Fig. 11c. Upon increasing the W/F ratio the conversion of ethane and yield of ethylene have increased. However, the selectivity towards ethylene has reached a maximum value at a W/F of 0.33 indicating the best operating parameters.

Cr/S.SBA-15 (highest activity material) catalyst was subjected to time on stream reaction (TOS) for 16 h, and the results are presented in Fig. 12. This catalyst showed steady catalytic activity up to 16 h of reaction time. Apart from ethylene we have also noticed the formation of CO, CH_4 and H_2 in the product gas. Both the catalysts have shown the same selectivity of $\cong$14% for methane, whereas the unmodified and sulfate-modified catalyst have shown variation in the CO (6.6 and 3.4%, respectively) and H_2 (1.7 and 0.7%, respectively) compositions. The higher values for the CO and H_2 shown by Cr/SBA-15 compared to that of Cr/S.SBA-15 may be due to over-oxidation of the main product ethylene, as reported in the earlier publication [5].

Conclusions

The sulfate-modified Cr/S.SBA-15 catalyst exhibits higher activity for the ODE with CO_2 compared to the unmodified catalyst. Sulfate modification affords higher dispersion of the Cr species. In both the catalysts, the Cr species exists in Cr^{6+} and Cr^{3+} states. The addition of sulfate ion to the support SBA-15 remarkably changes the redox properties of the CrO_x species. A higher Cr^{6+}/Cr^{3+} ratio is observed in the case of Cr/S.SBA-15 catalyst.

Acknowledgements The authors gratefully acknowledge the financial support to PSSP and KU by Council of Scientific and Industrial Research, New Delhi, India, under the Emeritus Scientist research scheme.

References

1. Karamullaoglu G, Dogu T (2007) Oxidative dehydrogenation of ethane over chromium–vanadium mixed oxide and chromium oxide catalysts. Ind Eng Chem Res 46:7079–7086
2. Lin X, Hoel CA, Sachtler WMH, Poeppelmeier KR, Weitz E (2009) Oxidative dehydrogenation (ODH) of ethane with O_2 as oxidant on selected transition metal-loaded zeolites. J Catal 265:54–62
3. Woods MP, Mirkelamoglu B, Ozkan US (2009) Oxygen and nitrous oxide as oxidants: implications for ethane oxidative dehydrogenation over silica–titania-supported molybdenum. J Phys Chem C 113:10112–10119

4. Ansari MB, Park SE (2012) Carbon dioxide utilization as a soft oxidant and promoter in catalysis. Energy Environ Sci 5:9419–9437
5. Ramesh Y, Thirumala Bai P, Hari Babu B, Lingaiah N, Rama Rao KS, Sai Prasad PS (2014) Oxidative dehydrogenation of ethane to ethylene on Cr_2O_3/Al_2O_3–ZrO_2 catalysts: the influence of oxidizing agent on ethylene selectivity. Appl Petrochem Res 4:247–252
6. Wang SB, Murata K, Hayakawa T, Hamakawa S, Suzuki K (2000) The catalytic activity in the dehydrogenation of ethane by CO_2. Dehydrogenation of ethane with carbon dioxide over supported chromium oxide catalysts. Appl Catal A 196:1–8
7. Nakagawa K, Okamura M, Ikenaga N, Suzuki T, Kobayashi T (1998) Dehydrogenation of ethane over gallium oxide in the presence of carbon dioxide. Chem Commun 9:1025–1026
8. Takahara I, Saito M (1996) Promoting effects of carbon dioxide on dehydrogenation of propane over a SiO_2-supported Cr_2O_3 catalyst. Chem Lett 25:973–974
9. Hong Y, Liwu L, Qingxia W, Longya X, Sujuan X, Shenglin L (2001) Studies in surface science and catalysis. In: Iglesia E, Spivey JJ, Fleisch TH (eds) Natural gas conversion VI. Elsevier, UK, pp 87–92
10. Mimura N, Okamoto M, Yamashita H, Oyama ST, Murata K (2006) Oxidative dehydrogenation of ethane over Cr/ZSM-5 catalysts using CO_2 as an oxidant. J Phys Chem B 110:21764–21770
11. Ge X, Zhu M, Shen J (2002) Catalytic performance of silica-supported chromium oxide catalysts in ethane dehydrogenation with carbon dioxide. React Kinet Catal Lett 77:103–108
12. Zhao X, Wang X (2010) Characterizations and catalytic properties of chromium silicalite-2 prepared by direct hydrothermal synthesis and impregnation. Catal Lett 135:233–240
13. Shi X, Ji S, Wang K, Li C (2008) Oxidative dehydrogenation of ethane with CO_2 over Novel Cr/SBA-15/Al_2O_3/FeCrAl monolithic catalysts. Energy Fuels 22:3631–3638
14. Wang S, Murata K, Hayakawa T, Hamakawa S, Suzuki K (1999) Oxidative dehydrogenation of ethane by carbon dioxide over sulfate-modified Cr_2O_3/SiO_2 catalysts. Catal Lett 63:59–64
15. Shaobin W, Murata K, Hayakawa T, Hamakawa S, Suzuki K (2001) Effect of promoters on catalytic performance of Cr/SiO_2 catalysts in oxidative dehydrogenation of ethane with carbon dioxide. Catal Lett 73:107–111
16. Wang S, Murata K, Hayakawa T, Hamakawa S, Suzuki K (1999) Oxidative dehydrogenation of ethane over sulfated zirconia supported oxides catalysts. React Kinet Catal Lett 67:219–224
17. Zhao D, Feng J, Huo Q, Melosh N, Fredrickson GH, Chmelka BF, Stucky GD (1998) Triblock copolymer syntheses of mesoporous silica with periodic 50 to 300 angstrom pores. Science 279:548–552
18. Zhang QH, Wang Y, Ohishi Y, Shishido T, Takehira K (2001) Vanadium-containing MCM-41 for partial oxidation of lower alkanes. J Catal 202:308–318
19. Shi X, Ji S, Wang K (2008) Oxidative dehydrogenation of ethane to ethylene with carbon dioxide over Cr–Ce/SBA-15 catalysts. Catal Lett 125:331–339
20. Esparza JM, Ojeda ML, Campero A, Domínguez A, Kornhauser I, Rojas F, Vidales AM, López RH, Zgrablich G (2004) N_2 sorption scanning behavior of SBA-15 porous substrates. Colloid Surf A Physicochem Eng Asp 241:35–45
21. Hari Krishna Charan P, Ranga Rao G (2013) Investigation of chromium oxide clusters grafted on SBA-15 using Cr-polycation sol. J Porous Mater 20:81–94
22. Zhang L, Zhao Y, Dai H, He H, Au CT (2008) A comparative investigation on the properties of Cr-SBA-15 and CrO_x/SBA-15. Catal Today 131:42–54
23. Mihaela M, Aurora R, Nicoleta C, Ion T, Vasile H (2010) Mesoporous silica functionalized with 1-furoyl thiourea urea for Hg(II) adsorption from aqueous media. J Hazard Mater 182:197–203
24. Oscar AA, Maria LM, Andrea RB (2009) Hydroxyapatite/MCM-41 and SBA-15 nano-composites: preparation, characterization and applications. Materials 2:1508–1519
25. Cherian M, Rao MS, Hirt AM, Wachs IE, Deo G (2002) Oxidative dehydrogenation of propane over supported chromia catalysts: influence of oxide supports and chromia loading. J Catal 211:482–495
26. Gaspar AB, Brito JLF, Dieguez LC (2003) Characterization of chromium species in catalysts for dehydrogenation and polymerization. J Mol Catal A 203:251–266
27. Jiménez-López A, Rodrigues-Castellón E, Maireles-Torres P, Díaz L, Mérida-Robles J (2001) Chromium oxide supported on zirconium- and lanthanum-doped mesoporous silica for oxidative dehydrogenation of propane. Appl Catal A 218:295–306
28. Derossi S, Ferraris G, Fremiotti S, Garrone E, Ghiotti G, Campa MC, Indovina V (1994) Propane dehydrogenation on chromia/silica and chromia/alumina catalysts. J Catal 148:36–46
29. Hakuli A, Kytökivi A, Krause AOI (2000) Dehydrogenation of i-butane on CrO_x/Al_2O_3 catalysts prepared by ALE and impregnation techniques. Appl Catal A 190:219–232
30. Cavani F, Koutyrev M, Trifiro F, Bartolini A, Ghisletti D, Iezzi R, Santucci A (1996) Chemical and physical characterization of alumina-supported chromia-based catalysts and their activity in dehydrogenation of isobutene. J Catal 158:236–250
31. Weckhuysen BM, Wachs IE, Schoonheydt RA (1996) surface chemistry and spectroscopy of chromium in inorganic oxides. Chem Rev 96:3327–3350
32. Grzybowska B, Slocynski J, Grabowski R, Wcislo K, Kozlowska A, Stoch J, Zielinski J (1998) chromium oxide/alumina catalysts in oxidative dehydrogenation of isobutane. J Catal 178:687–700
33. Hakuli A, Kytokivi A, Krause AOI, Suntola T (1996) Initial activity of reduced chromia/alumina catalyst inn-butane dehydrogenation monitored by on-line FT-IR gas analysis. J Catal 161:393–400
34. Thielemann JP, Ressler T, Walter A, Tzolova-Müller G, Christian H (2011) Structure of molybdenum oxide supported on silica SBA-15 studied by Raman, UV–Vis and X-ray absorption spectroscopy. Appl Catal A 399:28–34
35. Dines TJ, Inglis S (2003) Raman spectroscopic study of supported chromium (VI) oxide catalysts. Phys Chem Chem Phys 5:1320–1328
36. Vuurman MA, Stufkens DJ, Oskam A, Moulijn JA, Kapteijn F (1990) Raman spectra of chromium oxide species in CrO_3/Al_2O_3 catalysts. J Mol Catal 60:83–98
37. Yang S, Iglesia E, Bell AT (2005) Oxidative dehydrogenation of propane over $V_2O_5/MoO_3/Al_2O_3$ and $V_2O_5/Cr_2O_3/Al_2O_3$: structural characterization and catalytic function. J Phys Chem B 109:8987–9000
38. Wang Y, Ohishi Y, Shishido T, Zhang QH, Yang W, Guo Q, Wan HL, Takehira K (2003) Characterizations and catalytic properties of Cr-MCM-41 prepared by direct hydrothermal synthesis and template-ion exchange. J Catal 220:347–357
39. Takehira K, Ohishi Y, Shishido T, Kawabata T, Takaki K, Zhang Q, Wang Y (2004) Behavior of active sites on Cr-MCM-41 catalysts during the dehydrogenation of propane with CO_2. J Catal 224:404–416
40. Mimura N, Takahar I, Inaba M, Okamoto M, Murata K (2002) High-performance Cr/H-ZSM-5 catalysts for oxidative dehydrogenation of ethane to ethylene with CO_2 as an oxidant. Catal Commun 3:257–262
41. Fridman VZ, Xing R, Severance M (2016) Investigating the CrO_x/Al_2O_3dehydrogenation catalyst model: I. Identification and

stability evaluation of the Cr species on the fresh and equilibrated catalysts. Appl Catal A 523:39–53
42. Fridman VZ, Xing R (2017) Investigating the CrO_x/Al_2O_3 dehydrogenation catalyst model: II. Relative activity of the chromium species on the catalyst surface. Appl Catal A 530:154–165
43. Elmira A, Mohammad H, Farhad R (2016) CO_2-oxidative dehydrogenation of ethane to ethylene over Cr/MCM-41 nano catalyst synthesized via hydrothermal/impregnation methods: influence of chromium content on catalytic properties and performance. J Mol Catal A Chem 418–419:115–124